ROYAL SOCIETY
OF CHEMISTRY

PAPER

Check for updates

A novel polymer composite from polyhexamethylene guanidine hydrochloride for high performance triboelectric nanogenerators (TENGs)†

Doan T. Tung, [a] Le T. T. Tam, [ab] Nguyen T. T. Duong,[ab] Hoang T. Dung, [ab] Ngo T. Dung, [a] Nguyen A. Duc,[c] Phan N. Hong,[d] Nguyen T. Dung,[a] Phan N. Minh*[b] and Le T. Lu *[ab]

In this study, we report the successful fabrication of a novel antibacterial triboelectric nanogenerator (TENG) using a polymer composite film based on polyhexamethylene guanidine hydrochloride (PHMG). The composite materials, with optimised ingredient ratios, consist of PHMG, polyvinyl alcohol (PVA) and glutaraldehyde (GA) as a crosslinking agent (PHMG-GA-PVA). Utilising 3D printing, these composite materials were directly deposited on the conductive substrates and used as positive TENG electrodes. The obtained results show that the TENGs based on PHMG-GA-PVA exhibit high output efficiency, achieving peak-to-peak open-circuit voltage (V_{p-p}) and short-circuit current (I_{SC}) values of 664.5 V and 116.8 μA, respectively, at a low operating frequency of 1 Hz with an actuation force of 10 N. The device retains approximately 98% of its initial output voltage value after 360 000 contact-release cycles.

Introduction

Triboelectric nanogenerators are emerging as innovative devices for harvesting mechanical energy from various environmental sources and converting it into electricity. Over the past decade, the development of TENGs has mainly focused on enhancing the conversion efficiency of the devices through new structural designs and electrode materials.[1–4] To improve TENG performance, it is necessary to increase the charge density transferred during physical contact, as both open-circuit voltage and short-circuit current depend on the surface charge density. This density is predominantly influenced by the intrinsic properties of the materials used.[5,6]

The triboelectric effect is a universal phenomenon observed in most materials, including metals, wool, wood, and polymers.[7,8] Each material exhibits distinct triboelectric properties, influenced by its electron exchange capability, primarily determined by its chemical structure.[9–13] Polymers are the most commonly used materials in TENG electrodes. The functional groups present on these polymers play a crucial role in the contact electrification process.[14] Electron-withdrawing groups (*e.g.*, fluorine, chlorine, cyanide, ester, carboxyl and nitro), generally yield negative triboelectric properties.[15] In contrast, electron-donating groups (*e.g.* amidogen, amide, hydroxyl and alkoxy) tend to produce positive triboelectric properties.[15] In addition, some of the electric generation mechanisms in TENG when contacting different materials such as tribovoltaic nanogenerators (TVNG) and piezoelectric nanogenerator (PENG) have also been thoroughly explained in the literature.[16,17]

It has been demonstrated that polymers, such as thermoplastic polyurethane (TPU),[18,19] polypyrrole (PPy),[20,21] polyethylene oxide (PEO),[22,23] polybenzimidazole (PBI)[24] or polyvinyl alcohol (PVA)[25–27] with high mechanical properties, nitrogen-containing composition, or easy processability are commonly used as positive electrodes of TENGs. For example, Xin Jing *et al.* created a flexible semitransparent dual-electrode hydrogel-based TENG (DH-TENG) with high output when pairing a TPU tribopositive layer with a polydimethylsiloxane (PDMS) negative electrode. The device, achieving voltage of 311.5 V, current of 32.4 μA and a maximum power density of 2.7 W m^{-2}, can quickly charge capacitors and power small electronic devices.[18] PVA, a cost-effective polymer, is also frequently utilised in TENG application. Sannathammegowda *et al.* designed an economical PVA-TENG for mechanical energy harvesting. The uniform PVA membrane as positive friction electrode combined with a polypropylene (PP) negative friction electrode produced an open-circuit voltage V_{OC} and short-circuit current I_{SC} of 21.62 V and

aInstitute for Tropical Technology, Vietnam Academy of Science and Technology, 18 Hoang Quoc Viet, Hanoi, Vietnam. E-mail: ltlu@itt.vast.vn

bGraduate University of Science and Technology, Vietnam Academy of Science and Technology, 18 Hoang Quoc Viet, Hanoi, Vietnam. E-mail: pnminh@vast.vn

cDepartment of Physics, Faculty of Basic-Fundamental Sciences, Viet Nam Maritime University, 484 Lach Tray Road, Le Chan, Hai Phong, Vietnam

dCenter for High Technology Research and Development, Vietnam Academy of Science and Technology, 18 Hoang Quoc Viet, Hanoi, Vietnam

† Electronic supplementary information (ESI) available. See DOI: https://doi.org/10.1039/d4ra07768g

1.72 μA, respectively. The device also demonstrated mechanical durability and electrical stability over more than 5000 successful cycles. Furthermore, it also effectively charged commercial capacitors, digital clocks, and humidity sensors.[28]

In the current study, we introduce a novel polymer composite by combining PVA and polyhexamethylene guanidine hydrochloride (PHMG) – a cationic polymer containing amino and guanidine groups. PHMG not only exhibits high compatibility with various polymers but also possesses antimicrobial properties,[29–34] expanding its potential applications in medical and industrial fields.[35–40] The first use of PHMG for TENGs yielded promising results in triboelectric performance. The prepared device reveals a high peak-to-peak open-circuit voltage and peak-to-peak short-circuit current, with values of 664.5 V and 116.8 μA, respectively, at a low operating frequency of 1 Hz. In addition, the device exhibits a high durability, retaining appropriately 98% of its initial output voltage after 360 000 operational cycles. The results of this work could pave the way directions for the development of advanced renewable energy sources that meet the growing demand for clean and sustainable energy globally.

Experimental

Materials

Guanidine hydrochloride (GHC, CH_5N_3HCl 99%), hexamethylene diamine (HMDA, $C_6H_{16}N_2$ 99%), glutaraldehyde (GA) solution in H_2O (50 wt%) were purchased from Sigma-Aldrich (Singapore), polyvinyl alcohol 217 (PVA) was ordered from Kuraray-Poval (Singapore). All chemicals were used as received without any purification.

Copper adhesive tape with a thickness of 0.036 mm was ordered from 3 M company. Transparent Fluorinated ethylene propylene (FEP), with an approximately 0.15 mm thickness was purchased from Anycubic. White polyethylene terephthalate glycol (PETG) 3D printing filament is produced by Kingroon.

Preparing for PHMG-GA-PVA printing ink

PHMG was synthesised from GHC and HMDA monomers according to the following procedure: in a typical process, GHC and HMDA were weighed at molar ratio of 1 : 1 and added in a three-necked flask. The mixture was heated to 125 °C and maintained at this temperature for 4 h. The temperature was then increased to 160 °C and held for additional 4 h, followed by final rise to 180 °C for one hour before cooling to 60 °C. At this temperature, a certain amount of GA was added into the PHMG solution. The mixture was stirred for 2 h to form PHMG-GA. To prepare PHMG-GA-PVA composite, PVA is dissolved in double distilled water at a concentration of 5% by stirring at appropriately 90 °C. The PHMG-GA and PVA solutions were then mixed at the different mass ratios of PHMG-GA : PVA of 1 : 1; 4 : 1 and 8 : 1.

Fabrication of TENG electrode

The TENG PHMG-GA-PVA electrode was fabricated using 3D printing method. The PHMG-GA-PVA gel was directly printed onto 10×10 cm² copper adhesive tape. The printing parameters, including a speed of 20 mm min⁻¹, line width of 0.6 mm, layer thickness of 0.2 mm and substrate temperature of 80 °C were determined. The described 3D printing technique employs a dual-pass method with orthogonal infill patterns. In the initial pass, the printer deposits material along a predetermined axis, creating a series of parallel lines. The second pass then applies material in a direction perpendicular to the first, resulting in a cross-hatched internal structure. After printing, the electrodes were dried in an oven at a temperature of 120 °C overnight. The fabrication process of PHMG-GA-PVA TENG electrode is presented in Fig. 1.

Structure of TENG device

The TENG device consists of three 3D-printed parts made from PETG filament. The top and bottom components incorporate PHMG-GA-PVA printed electrodes, which serve as positive friction electrodes, while the middle component has two symmetrical sides mounted on the FEP membrane to act as a negative friction electrode. Rubber buttons, commonly used in computer keyboards, were used to separate the electrodes.

Characteristics

FTIR spectra were recorded using a Nicolet 6700 FT-IR spectrometer in the wavenumber range of 4000–400 cm⁻¹. A field
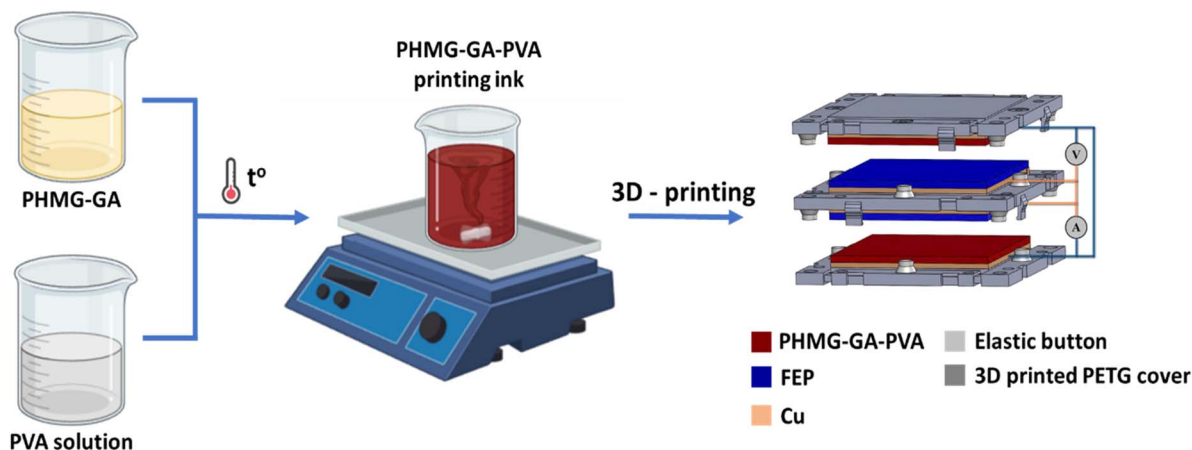

Fig. 1 Illustration of the fabrication process for PHMG–GA–PVA TENG electrodes.

emission scanning electron microscope (FE-SEM, HITACHI) equipped with an energy dispersive X-ray spectroscope (EDX) was used to investigate the morphology and elemental composition of the TENG electrode.

The open-circuit voltages (OCV or V_{OC}) of the TENG device were characterised using Lecroy Wave Surfer 424 oscilloscope. The short-circuit currents (I_{SC}) of the device were amplified by a low-noise current preamplifier SR570 and measured with a Tektronix DPO4032 oscilloscope.

Mechanical properties were determined by two parameters: impact strength and bending strength. Impact strength was measured using ERICHSEN Impact Tester 304 according to ISO 6272-1 standard. Bending strength was performed using the ELCOMETER 1500 on-axis flexural tester according to ASTM-D522 standard.

The evaluation of the antibacterial efficacy of the PHMG-containing membrane samples coated on copper substrates was conducted using the colony method as follows: initially, the sample (2 cm × 2 cm) was placed on a Petri dish containing 0.4 mL of *E. coli* (Gram-negative bacteria) or *B. subtilis* (Gram-positive bacteria) at a density of $\sim 10^8$ CFU mL^{-1} and left in contact for 1 hour. The sample was then removed and shaken in 20 mL of 0.9% NaCl solution for 2 minutes. The resulting liquid was diluted 100 times with saline solution. A volume of 100 μL from this dilution was transferred onto Luria-Bertani agar plates, which were then placed in a climate-controlled incubator set at 37 °C for 24 hours. The plates were then carefully examined to identify or count the colonies that had grown on the agar surface. In addition, the PHMG-coated copper membrane was also soaked in double distilled water for 15 minutes before performing the antibacterial test to evaluate the effect of water on the washout of the PHMG membrane.

Results and discussions

Polymer composite material property

Chemical compositions of the materials are characterised using FTIR analysis. Fig. 2 shows FTIR spectra of PVA, PHMG, PHMG-GA and PHMG-GA-PVA prepared at the PHMG-GA : PVA ratio of
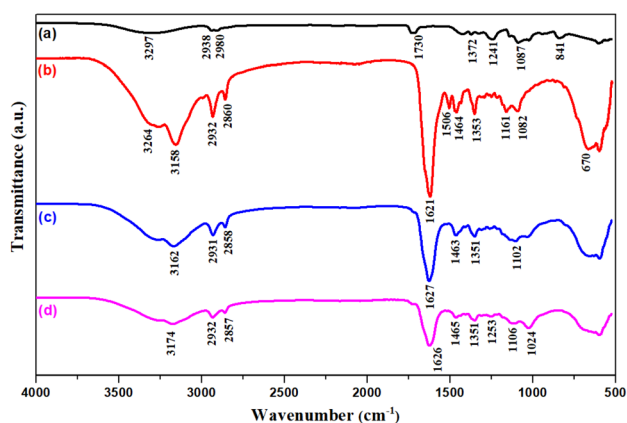
Fig. 2 FTIR spectra of PVA (a), PHMG (b), PHMG-GA (c), and PHMG-GA-PVA (at the ratio of 8 : 1) (d).

8 : 1. The characteristic peaks of pure PVA (a) used in this study are shown by two strong absorption bands at wavenumbers 1241 cm^{-1} (C–O–C) and 1087 cm^{-1} (C–OH), indicating that PVA retains some acetate groups and –OH groups along the polymer chain. The infrared (IR) spectrum of PHMG (b) shows bands at 3158 cm^{-1} and 1464 cm^{-1}, which are assigned to N–H stretching and bending vibrations of a secondary amine group, respectively. Two absorption peaks at 2932 cm^{-1} and 2860 cm^{-1} are characteristic of symmetric and asymmetric stretching vibrations of the CH$_2$ group. The peak at 1621 cm^{-1} is attributed to the C=N bond. The band at 1353 cm^{-1} is characteristic of the C–N bond stretching of the secondary amine group. The absorption peaks at 3264 cm^{-1} and 1160 cm^{-1} are assigned to O–H stretching and bending vibrations, respectively. The IR spectrum of the PHMG-GA (c) membrane exhibits a characteristic absorption peak of GA at 1100 cm^{-1}, which is assigned to the C=O bond stretching vibration.[41] The IR spectrum of the PHMG-GA/PVA (d) membrane exhibits a characteristic absorption peak of PVA at 3297 cm^{-1}, which is assigned to the O–H bond stretching vibration of the hydroxyl group. Additionally, two peaks at 1253 cm^{-1} (C–O–C) and 1024 cm^{-1} (C–OH) characteristic of PVA, are still present, indicating the presence of PVA in the PHMG-GA-PVA composition.

Fig. 3 shows the SEM, EDX, and EDX mapping images of the printed polymer electrode composed of PHMG, cross-linking agent GA, and PVA. The SEM image reveals a relatively smooth surface with microstructures and layered printing, reflecting the 3D printing process with sequentially stacked polymer layers. The EDX results identify the presence of elements within the material, with spectral peaks corresponding to the characteristic elements of PHMG (*e.g.*, carbon, chlorine, nitrogen), GA (*e.g.*, oxygen, carbon), and PVA (*e.g.*, carbon, oxygen). Quantitative analysis indicates the relative proportions of these elements, where a higher carbon and oxygen content is expected due to the polymeric nature of the components. The EDX mapping analysis provides a detailed view of the distribution of the elements within the sample. The mapping images show each color representing a different element, highlighting areas where specific elements are concentrated. For instance, a uniform distribution of carbon is expected as all components contain carbon, while oxygen-rich areas correspond to PVA or GA. Furthermore, the presence of nitrogen indicates regions rich in PHMG.

Triboelectric properties

To evaluate the triboelectric properties of PHMG, five TENG electrode materials, including pure PVA and PVA with varying PHMG ratios were investigated. Fig. 4 indicates the output open-circuit voltage of the device under the same applied force. It can be seen that the pure PVA electrode generates the lowest voltage, with a positive value of about 181 V and a negative value of around −79 V, indicating the limited electrical generation capacity (Fig. 4a). As the PHMG ratio increases, the electrical performance also improves significantly. For example, at the ratio of PHMG-GA/PVA = 1 : 1 (PHMG1-GA-PVA1) the sample achieves a maximum positive voltage of approximately 215 V
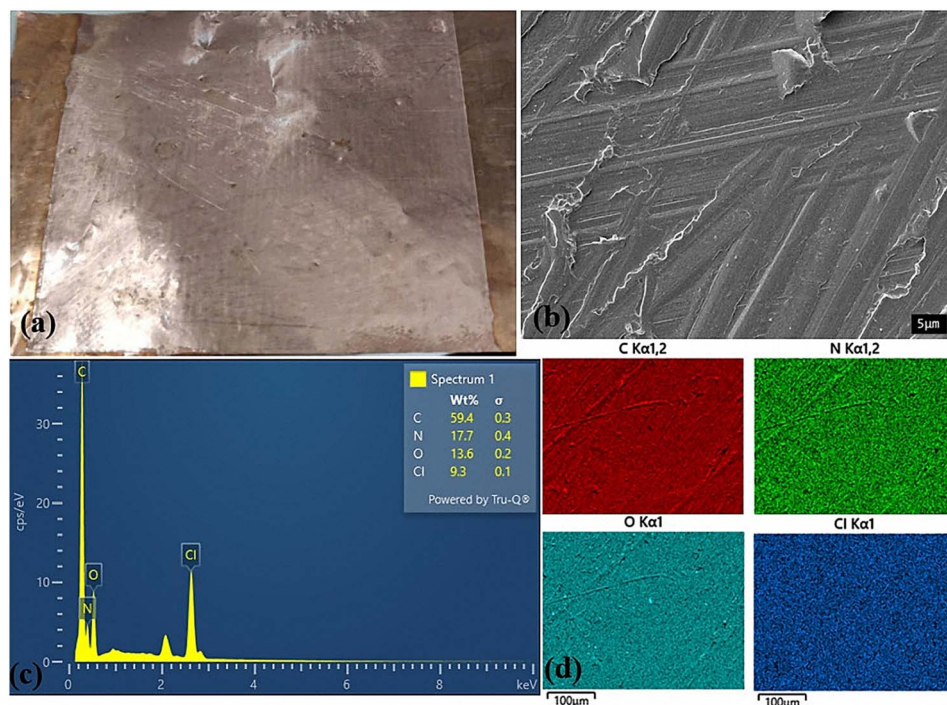
Fig. 3 (a) Appearance photo, (b) SEM, (c) EDX and (d) EDX mapping of the 3D-printing PHMG-GA-PVA electrode prepared at PHMG-GA : PVA ratio of 8 : 1.

and a negative voltage of around −118 V, while it reaches 387 V (positive) and −137 V (negative) for the ratio of 4 : 1 (PHMG4-GA-PVA1). These values reach 462 V (positive) and −199 V (negative) at the ratio of 8 : 1 (PHMG8-GA-PVA1).

Notably, the PHMG-GA sample without PVA achieves the highest voltages, reaching a maximum positive value of around 494 V and a negative value of approximately −230 V. However, the absence of PVA significantly impacts PHMG's film-forming ability, making it relatively less durable. PHMG tends to form discrete clusters and lacks the ability to form cross-links or stable molecular networks. As a result, during the printing

process, the material did not flow evenly and continuously, leading to uneven or interrupted print lines. The resulting film often has cracks, small holes or uneven surfaces and needs a long drying time. In the current study, GA serves as a linker to enhance the structural and mechanical properties of the material.

Fig. 4b and Table 1 show a trend of OCV values changing with the mass percentage of PHMG. It is clear that OCV values increase with the increasing PHMG content. PHMG is a polymer containing guanide reactive groups ($=NH$), which can interact with H+ to form cations ($=NH^+$). These active groups carry
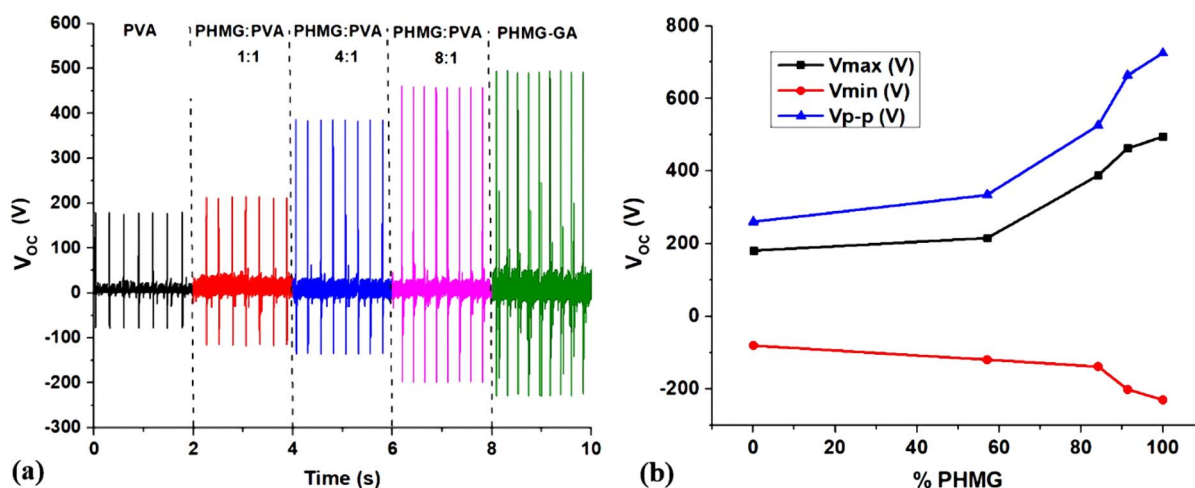

Fig. 4 (a) Open circuit voltages (V_{OC}) of PVA, PHMG-GA-PVA and PHMG-GA electrodes prepared at different ratios of PHMG-GA/PVA; (b) maximum (V_{max}), minimum (V_{min}), and peak-to-peak (V_{p-p}) voltages of V_{OC} as a function of PHMG content.

Table 1 OCV values of PHMG-GA-PVA samples

Samples	V_{max} (V)	V_{min} (V)	V_{p-p} (V)
PVA	181	−79	260
PHMG1-GA-PVA1	215	−118	333
PHMG4-GA-PVA1	387	−137	524
PHMG8-GA-PVA1	462	−199	661
PHMG-GA	494	−230	724

a positive charge, making PHMG a highly efficient positive tribopolymer. The addition of PVA as a binding agent significantly improves film-forming ability by enhancing intermolecular interactions, thereby improving flexibility and the mechanical strength of the films. Table S1† further compares the maximum generated triboelectric voltage values with other publications showing the role of the new positive friction material PHMG.

To evaluate the triboelectric properties in more detail, PHMG8-GA-PVA1 sample was selected. Fig. 5 indicates the influence of working frequency on the open circuit voltage (OCV) and short circuit current (I_{SC}). At low operating frequencies (1–5 Hz), the voltage (V_{p-p}) remains around 664 V, almost unchanged as the operating frequency increase (Table 2). However, the V_{p-p} value decreases at higher operating frequencies (10 and 20 Hz). According to the basic theory of a contact-separation TENG system, we have the equation:[42,43]

$$V_{oc} = -\frac{Q}{S\varepsilon_0}\left(\frac{d_1}{\varepsilon_1} + \frac{d_2}{\varepsilon_2} + x(t)\right) + \frac{\sigma x(t)}{\varepsilon_0} \quad (1)$$

where Q is the amount of charge transferred (C), and x is the distance that can be moved between the two friction charge layers, ε_0, S and σ are the dielectric constant of vacuum, the working area of the friction electrode and the static charge density on the friction layer, respectively. Additionally, d_1 and d_2 are the thicknesses, and ε_1 and ε_2 are the relative dielectric constants of the two friction material layers (PHMG-GA-PVA and FEP). With two boundary conditions, open circuit voltage ($Q = 0$) and short circuit current (V = 0) and by setting $d_o = d_1/\varepsilon_1$

$+ d_2/\varepsilon_2$, we can easily obtain the following two corresponding equations:

$$V_{oc} = \frac{\sigma x(t)}{\varepsilon_0} \quad (2)$$

$$I_{sc} = \frac{dQ_{sc}}{dt} = \frac{S\sigma d_0}{[d_0 + x(t)]^2}\frac{dx}{dt} = \frac{S\sigma d_0 v(t)}{[d_0 + x(t)]^2} \quad (3)$$

where, $v(t)$ is the impact movement speed between the two electrode plates of the TENG module.

From eqn (2), it can be seen that the open circuit voltage is independent of the operating frequency. Therefore, in theory, V_{OC} should not change with frequency. This is consistent with the experimental data at low working frequencies (1–5 Hz), as shown in Table 2. However, the experimental data indicate a decrease in V_{OC} at frequencies above 10 Hz. At high frequencies, the reduction in V_{OC} values is possible due to the fact that the impact speed is faster than the recovery time to the initial state of the electrode.[44]

In addition, according to eqn (3), it can be seen that the short-circuit current I_{SC} is expected to increase with the impact frequency. If the moving speed of the two TENG electrodes is considered constant, the frequency will be proportional to $v(t)$. Thus, a higher frequency corresponds to a larger $v(t)$. This increase in short-circuit current (I_{sc}) with the impact frequency was observed experimentally, as shown in Fig. 5 and Table 2. From Table 2, it is evident that the I_{sc} values of the TENG device utilising the positive electrode material of PHMG8-GA-PVA1 are relatively high compared to some other reports using PVA electrode material.[28]

As a device that converts mechanical movement into electricity, stability during operation is crucial for practical applications. In this study, a durability test was conducted at an impact frequency of 20 Hz and the results shown in Fig. 6a. The output voltage decreases insignificantly (by only 2%) after 360 000 working cycles suggesting that the device can maintain a stable output for an extended period in practical applications. To demonstrate the applicability of the TENG device utilising PHMG-GA-PVA electrode, we connected it with LED systems. As
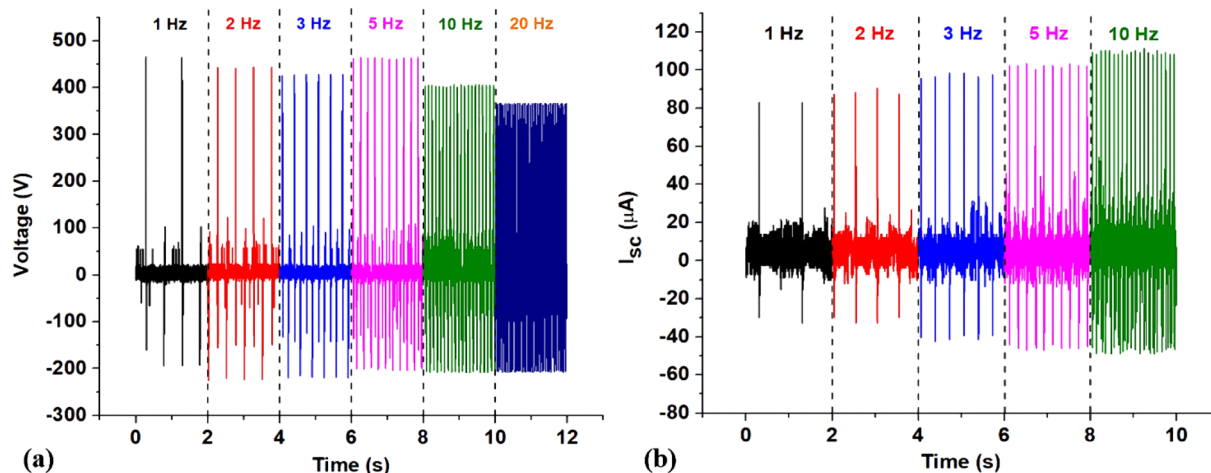

Fig. 5 V_{oc} (a) and I_{sc} (b) values at the different working frequencies of PHMG8-GA-PVA1 electrode.

Table 2 V_{OC} and I_{SC} values of the device utilising PHMG8-GA-PVA1 electrode at the different impact frequencies

Frequency (Hz)	V_{max} (V)	V_{min} (V)	V_{p-p} (V)	I_{max} (μA)	I_{min} (μA)	I_{p-p} (μA)
1	467.4	−197.1	664.5	84.0	−32.8	116.8
2	443.1	−225.2	668.3	90.4	−32.8	132.2
3	433.0	−223.1	656.1	98.4	−42.4	140.8
5	462.4	−205.9	668.3	103.2	−47.2	150.4
10	403.5	−208.7	611.2	111.2	−48.8	160.0
20	364.7	−207.3	572.0	119.8	−52.6	172.4

shown in Fig. 6b, all LEDs were lit under full daylight conditions. Additionally, when measuring impact resistance, a 2 kg metal ball dropped from a height of 100 cm showed that the film did not crack or peel off from the copper substrate (Fig. S1a†). In the bending strength test (Fig. S1b†), the film also did not crack or peel off the copper substrate when bent around the smallest diameter axis of the Elcometer 1500 device (2 mm). Therefore, the PHMG8-GA-PVA1 film can be aimed at applications for flexible wearable devices.

Finally, the antibacterial properties of the PHMG8-GA-PVA1 membrane were evaluated, with the results shown in Fig. S2.† PHMG, PHMG-GA, and PHMG8-GA-PVA1 all showed good antibacterial properties, even at a high initial bacterial density of 10^8 CFU mL^{-1}. After soaking in water for 15 minutes, PHMG without GA was partially hydrolyzed in water and its antibacterial ability was reduced (shown by the appearance of both *S. subtilis* (gram +) and *E. coli* (gram −) colonies on the agar surface in the Petri dish). However, when the GA crosslinking agent was present, the membrane exhibited better structural integrity and increased water-resistant. With its strong antibacterial ability, the PHMG8-GA-PVA1 membrane shows great potential for use in antibacterial facemasks and self-deodorized smart shoes.

Conclusions

For the first time, PHMG material-a polymer with strong antibacterial properties, has been successfully utilized in a TENG device as a positive electrode. The results indicate that the PHMG content in the positive electrode affects the output of the TENG device. The presence of amine functional groups of the PHMG combined with GA as cross-linker and PVA enables the device to achieve impressive triboelectric performance, with a peak-to-peak open-circuit voltage of up to 664.5 V and a short-circuit current of 116.8 μA at a low operating frequency of 1 Hz when using a PHMG-GA : PVA ratio of 8 : 1. At a higher frequency of 20 Hz, the device maintains and output of 572 V and 172 μA under an actuation force of 10 N. Furthermore, the device retains appropriately 98% of its initial output voltage after 360 000 operational cycles, suggesting its potential for practical applications such as self-powered devices, sensors, and particularly in antibacterial facemasks and self-deodorized smart shoes.
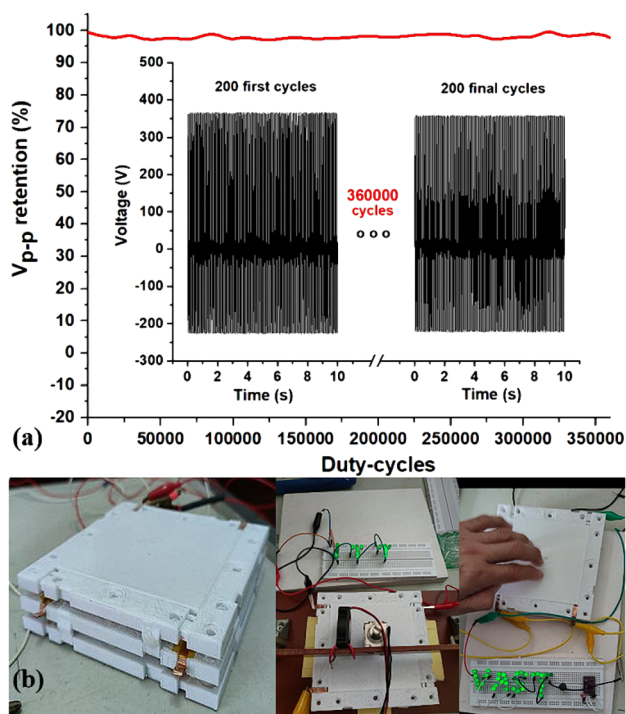
Data availability

All data supporting the findings of this study are included within the manuscript and as part of the ESI.†

Author contributions

Doan T. Tung and Nguyen T. Dung prepared the PHMG-GA-PVA 3D printing solution; Le T. T. Tam synthesised PHMG and performed SEM-EDX analysis; Nguyen T. T. Duong conducted FTIR analysis; Hoang T. Dung designed the printing patterns, electrodes, and TENG device; Ngo T. Dung performed 3D printing and post-processing of TENG electrodes; Nguyen A. Duc and Phan N. Hong carried out triboelectric characterization; Phan N. Minh and Le T. Lu provided scientific guidance and supervision. All authors contributed to writing and revising the manuscript.

Fig. 6 Output voltage decline of a 3D printed PHMG-GA-PVA TENG device after 360 000 working cycles (a) and photos of a TENG module used to power for LEDs (b).

Conflicts of interest

The authors declare that they have no competing interests.

Acknowledgements

References

1 J. Si, R. Duan, M. Zhang and X. Liu, *Nanomaterials*, 2022, **12**, 1385.

2 W. G. Kim, D. W. Kim, I. W. Tcho, J. K. Kim, M. S. Kim and Y. K. Choi, *ACS Nano*, 2021, **15**(1), 258–287.

3 Y. Li, Y. Luo, H. Deng, S. Shi, S. Tian, H. Wu, J. Tang, C. Zhang, X. Zhang, J. W. Zha and S. Xiao, *Adv. Mater.*, 2024, 2314380.

4 M. M. Rastegardoost, O. A. Tafreshi, Z. Saadatnia, S. Ghaffari-Mosanenzadeh, C. B. Park and H. E. Naguib, *Nano Energy*, 2023, **111**, 108365.

5 V. A. Cao, S. Lee, M. Kim, M. M. Alam, P. Park and J. Nah, *Nano Energy*, 2020, **67**, 104300.

6 R. L. Bulathsinghala, A. Ravichandran, H. Zhao, W. Ding and R. Dharmasena, *Nano Energy*, 2024, **123**, 109383.

7 A. F. Yu, Y. X. Zhu, W. Wang and J. Y. Zhai, *Adv. Funct. Mater.*, 2019, **29**, 1900098.

8 X. Zhang, Y. Zhang, J. Zhang, J. Shang, L. Lin, Q. Liu and Q. An, *Chem. Eng. J.*, 2024, **483**, 149314.

9 S. M. Hsu and R. S. Gates, *J. Phys. D: Appl. Phys.*, 2006, **39**, 3128.

10 Y. Wang, N. Yamada, J. Xu, J. Zhang, Q. Chen, Y. Ootani, Y. Higuchi, N. Ozawa, M.-I. D. B. Bouchet, J. M. Martin, S. Mori, K. Adachi and M. Kubo, *Sci. Adv.*, 2019, **5**, eaax9301.

11 C. A. Mizzi, A. Y. W. Lin and L. D. Marks, *Phys. Rev. Lett.*, 2019, **123**, 116103.

12 H. Ko, Y. W. Lim, S. Han, C. K. Jeong and S. B. Cho, *ACS Energy Lett.*, 2021, **6**, 2792–2799.

13 D. Kang, H. Y. Lee, J.-H. Hwang, S. Jeon, D. Kim, S. Kim and S.-W. Kim, *Nano Energy*, 2022, **100**, 107531.

14 S. Li, J. Nie, Y. Shi, X. Tao, F. Wang, J. Tian, S. Lin, X. Chen and Z. L. Wang, *Adv. Mater.*, 2020, **32**, 2001307.

15 A. Chen, C. Zhang, G. Zhu and Z. L. Wang, *Adv. Sci.*, 2020, **7**, 2000186.

16 Z. Liu, S. Lin, P. Yang, S. Qin, J. Hun and X. Chen, *Energy Environ. Sci.*, 2024, **17**, 6582–6593.

17 S. Qin, J. Chen, P. Yang, Z. Liu, X. Tao, X. Dong, J. Hu, X. Chu, Z. L. Wang and X. Chen, *Adv. Energy Mater.*, 2024, **14**, 2303080.

18 X. Jing, H. Li, H. Y. Mi, P. Y. Feng, X. Tao, Y. Liu, C. Liu and C. Shen, *J. Mater. Chem. C*, 2020, **8**, 5752.

19 H. Joo, S. Gwak, M. H. Lee, H. Park, C. Lee, J. H. Lee, S. A Han and J. H. Lee, *Sustainable Mater. Technol.*, 2023, **36**, e00638.

20 H. Zhang, P. Zhang, L. Deng, W. Zhang, B. Liu, D. Ren and Z. Yang, *ACS Appl. Nano Mater.*, 2022, **5**(8), 11219–11228.

21 Q. Tang, Q. Ke, Q. Chen, X. Zhang, J. Su, C. Ning and L. Fang, *ACS Appl. Mater. Interfaces*, 2023, **15**(14), 17641–17652.

22 P. Ding, J. Chen, U. Farooq, P. Zhao, N. Soin, L. Yu, H. Jin, X. Wang, S. Dong and J. Luo, *Nano Energy*, 2018, **46**, 63–72.

23 Z. Qian, R. Li, J. Guo, Z. Wang, X. Li, C. Li, N. Zhao and J. Xu, *Nano Energy*, 2019, **64**, 103900.

24 X. Tao, P. Yang, Z. Liu, S. Qin, J. Hu, Z.-X. Huang, X. Chen and J.-P. Qu, *ACS Nano*, 2024, **18**(5), 4467–4477.

25 S. Wang and Y. Zhang, *Mater. Technol.*, 2022, **37**(13), 2752–2757.

26 I. C. M. Candido, G. S. Oliveira, S. J. L. Ribeiro, M. Cavicchioli, H. S. Barud, L. G. Silva and H. P. de Oliveira, *Nano Energy*, 2023, **105**, 108035.

27 S. Yempally, J. J. Cabibihan and D. Ponnamma, *Energy Technol.*, 2024, **12**, 2300992.

28 S. Amini, R. F. S. M. Ahmed, S. M. Ankanathappa and K. Sannathammegowda, *Nanotechnology*, 2023, **35**(3), 035403.

29 D. T. Nguyen, L. T. Pham, H. T. T. Le, M. X. Vu, H. T. M. Le, H. T. M. Le, N. H. Pham and L. T. Lu, *RSC Adv.*, 2018, **8**, 19707–19712.

30 J. Chen, D. Wei, W. Gong, A. Zheng and Y. Guan, *ACS Appl. Mater. Interfaces*, 2018, **10**(43), 37535–37543.

31 S. Chen, C. Li, T. Hou, Y. Cai, L. Liang, L. Chen and M. Li, *React. Funct. Polym.*, 2019, **145**, 104379.

32 Q. Lin, L. Wu, W. Hu, X. Wan, Z. Wu and C. Zhang, *Surf. Interface*, 2022, **29**, 101708.

33 B. Qiu, M. Wang, W. Yu, S. Li, W. Zhang, S. Wang and J. Shi, *Polymers*, 2023, **15**, 1521.

34 Y. Zhao, D. Wei, X. Xu and Y. Guan, *Polym. Advan. Technol.*, 2024, **35**, e6314.

35 M. Sahraro, H. Yeganeh and M. Sorayya, *Mater. Sci. Eng. C*, 2016, **59**, 1025–1037.

36 H. Choi, K. J. Kim and D. G. Lee, *Fungal Biol.*, 2017, **121**(1), 53–60.

37 C. Zhang, Z. Ying, Q. Luo, H. Du, Y. Wang, K. Zhang, S. Yan, X. Li, Z. Shen and W. Zhu, *J. Polym. Sci., Part A: Polym. Chem.*, 2017, **55**, 2027–2035.

38 Y. Zhu, Y. Gu, S. Qiao, L. Zhou, J. Shi and H. Lai, *J. Biomed. Mater. Res., Part A*, 2017, **105**, 871–878.

39 S. Zhang, D. Wei, X. Xu and Y. Guan, *Coatings*, 2023, **13**, 1115.

40 W. Y. Wang, H. W. Hu, J. C. Chiou, K. F. Yung and C. W. Kan, *Polym. Chem.*, 2023, **14**, 5226–5252.

41 H. Hu, J. H. Xin, H. Hu, A. Chan and L. He, *Carbohydr. Polym.*, 2013, **91**(1), 305–313.

42 S. Niu, S. Wang, L. Lin, Y. Liu, Y. S. Zhou, Y. Hu and Z. L. Wang, *Energy Environ. Sci.*, 2013, **6**(12), 3576–3583.

43 S. Hu, J. Han, Z. Shi, K. Chen, N. Xu, Y. Wang, R. Zheng, Y. Tao, Q. Sun, Z. L. Wang and G. Yang, *Nano-Micro Lett.*, 2022, **14**, 115.

44 H. T. Deng, Z. Y. Wang, Y. L. Wang, D. L. Wen and X. S. Zhang, *Microsyst. Nanoeng.*, 2022, **8**, 61.